Bull. Mater. Sci., Vol. 34, No. 7, December 2011, pp. 1591–1597. © Indian Academy of Sciences.

Hot pressing effect on $(Bi_{0.25}Sb_{0.75})_2Te_3$ mechanical and thermoelectric properties

G KAVEI*, K AHMADI and A SEYYEDI†

Material and Energy Research Centre, P.O. Box 14155-4777, Tehran, Iran
†Payam Nour University, Lashkarak, Ozgol, Tehran, Iran

MS received 18 April 2010

Abstract. **$(Bi_{0.25}Sb_{0.75})_2Te_3$ thermoelectric material is a well known *p* type of compound that has higher figure of merit than other stoichiometries. The crystal of this compound was prepared, pulverized in a particle size ratio of 64% with a mesh of 80 (200 μm^2) and 36% with a mesh of 60 (250 μm^2). The powder was sintered in a heat up to 350–500°C under pressure of 500 MPa (hot pressing). To find out the temperature effects on thermal conductivity of the sample it was systematically investigated in nano-scale intrinsic structures by systems of X-ray diffraction, scanning electron microscopy and, for only once successful attempt, atomic force microscopy. The acquired images ensured to show homogeneous structures for hot pressed samples. In terms of thermal conductivity and with regard to the figure of merit (*Z*), optimum sintering temperature hovers at around 500°C, which leads to a maximum *Z* value of around 1·53 K^{-1}.**

Keywords. **Sinter; longitudinal; transverse; hot pressing; thermal conductivity; scanning probe microscopy.**

1. Introduction

Single and polycrystalline $(Bi_2Te_3)_x(Bi_2Se_3)_{1-x}$ alloys have been extensively investigated as *p*-type materials for Peltier coolers and thermoelectric generators if and when they are used at nearly room temperature. The thermoelectric figure of merit was found to be optimum as crystal has $(Bi_{0.25}Sb_{0.75})_2Te_3$ stoichiometry (Scherrer and Scherrer 1995; Ohsugi *et al* 1990).

At present, there are several fabrication methods to improve cooling and mechanical properties of bismuth telluride-based compounds. One of these methods is that of unidirectional crystal growth which usually increases thermoelectric properties (Hyun *et al* 2001; Kitagawa *et al* 2003). However, this process usually lasts long and their products are mechanically weak. To improve mechanical properties of the elements, several methods have been proposed, one example of which is pulverization (Liu and Park 2002; Park *et al* 2002). For this purpose, polycrystalline $(Bi_{0.25}Sb_{0.75})_2Te_3$ was fabricated by mechanically alloying and then by hot pressing (Oh *et al* 2000). As an alternative, thermoelectric material could be prepared with a solid solution and through crystallization followed by pulverizing and hot pressing (Keawprak *et al* 2005). The induced impurities in fabrication process behave like donors and influence the thermoelectric properties of the compound (Wada *et al* 1991).

*Author for correspondence
(g-kavei@merc.ac.ir, prof.kavei@hotmail.com)

The present study discusses thermal conductivity, other thermoelectric parameters and mechanical properties of fabricated $(Bi_{0.25}Sb_{0.75})_2Te_3$ compound which was hot pressed and sintered at 350, 425 and 500°C.

2. Experimental

A cylindrical rod of *p*-type thermoelectric crystals of $(Bi_{0.25}Sb_{0.75})_2Te_3$ was prepared the same way as described in Kavei and Karami (2006). The rod was crushed in an agate mortar and pestle. The alloy powder to a particle size ratio of 64% with a mesh of 80 (200 μm^2) and 36% with a mesh of 60 (250 μm^2) was obtained. Several powders weighing 2·1 g were pressed under 500 MPa compressive pressure stress in a steel mold and samples of size, $5 \times 5 \times 10$ mm^3 were obtained. These samples were sintered at sintering temperatures of 350, 425 and 500°C under 500 MPa compressive pressure for a period of 10 min. Sintering condition including an axial pressure of 500 MPa and a sintering time of 10 min was tentatively obtained as optimally as possible. Such a slow rate of sintering avoids internal stress and micro cracks which leads to perfect compact crystallites (surface to core). This was confirmed by AFM images. The density of the samples at each stage of hot pressing was measured as listed in table 1. Although the pressure force as applied in this study was much higher than that in Keawprak *et al* (2005), however, obtained values for density were lower. This could be due to larger particle size in our experiments. From the crystal densities of 7·74 g cm^{-3} for Bi_2Te_3 and 6·5 g cm^{-3} for Sb_2Te_3 (Lide 2008), the expected

Table 1. Typical results of Seebeck coefficients, electrical conductivity and thermal conductivity were measured in longitudinal direction of selected samples pressed at 500 MPa and three different temperatures for sintering time of 10 min. The results were compared with those mentioned in Keawprak *et al* (2005).

	Longitudinal					
Parameters	Present study, press at 500 MPa, sintering time 10 min				(Keawprak *et al* 2005), press at 75 MPa, sintering time, 10 min	
T (°C)	350	425	500	345	445	495
α (μV K^{-1})	225	225	235	235	235	212
σ_H (Ω cm^{-1})	452	523	533	325	450	650
κ (W mK^{-1})	1·37	1·46	1·53	0·6	0·78	1·00
$Z = \alpha^2\sigma/\kappa \times 10^{-3}$ (K^{-1})	1·67	1·82	1·92	2·99	3·2	2·92
d (g cm^{-3})	6·43	6·54	6·71	6·52	6·81	6·81

crystal density for $(Bi_{0·25}Sb_{0·75})_2Te_3$ was 6·81 g cm^{-3}. Therefore, the density values given in Keawprak *et al* (2005) seem to be too high for powder samples implying that our results are relatively accurate than those quoted in Keawprak *et al* (2005).

A number of characterizations were carried out under longitudinal and transverse directions. Longitudinal and transverse directions refer to those directions that are parallel and perpendicular to a direction to which a sample is pressed, respectively.

Phase identification of the sintered compacts was examined by X-ray diffraction (XRD) in a Philips X'pert-system. In order to obtain a reference sample for the XRD profiles, some crushed powder was milled with ball-milling technique. Fractured surfaces of sintered material in longitudinal and transverse sections were examined using a Cambridge-30S scanning electron microscope (SEM) and scanning probe microscopy (SPM) system at NC–AFM mode.

Thermal conductivity (κ) of the samples at different sintering temperatures was measured along the longitudinal direction by a device designed in our laboratory. Additional details of the device can be obtained in Kavei *et al* (2008a). In spite of extensive attempts, thermal conductivity measurements in transverse mode was not successful because of small sample size (5 mm). Density of the samples was measured based on Archimedes experiment by means of a balance system (Mettler–Toledo Model AG285) to obtain thermal conductivity via $\kappa = dC_p\kappa_d$ and compare the results with values published in Keawprak *et al* (2005). Finally figure of merit ($Z = \alpha^2\sigma/\kappa$) was calculated for sintering temperature ranges as mentioned above.

3. Results and discussion

The results have been analysed on the following two physical bases.

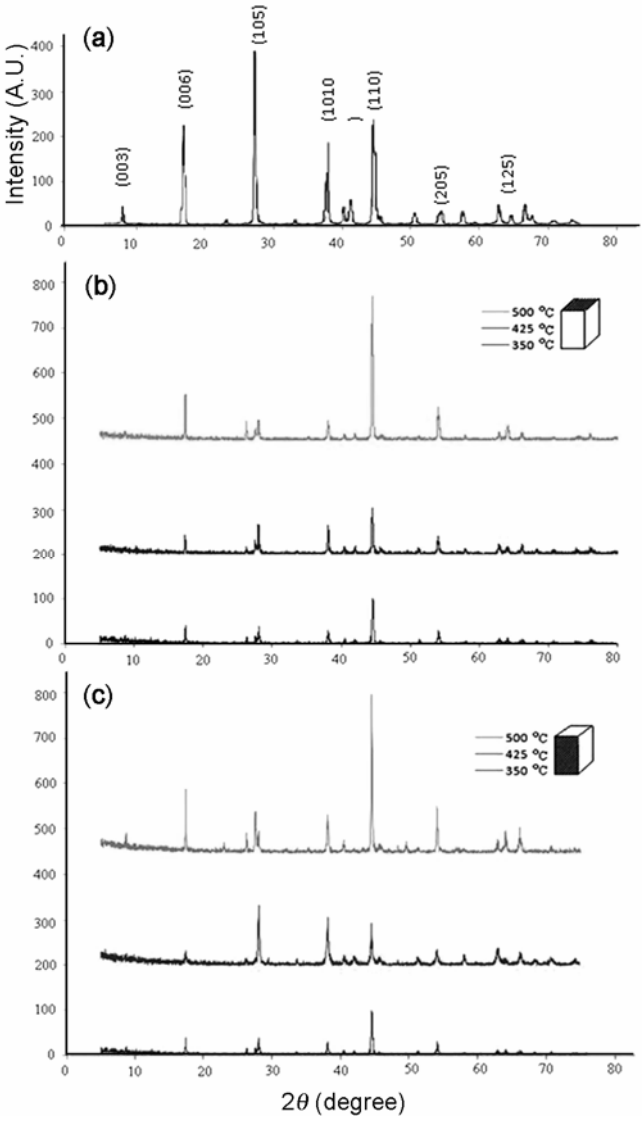

Figure 1. XRD patterns from (**a**) powdered $(Bi_{0·25}Sb_{0·75})_2Te_3$ compound as a reference, (**b**) transverse and (**c**) longitudinal sections of samples sintered at typical (350, 425 and 500°C) sintering temperatures.

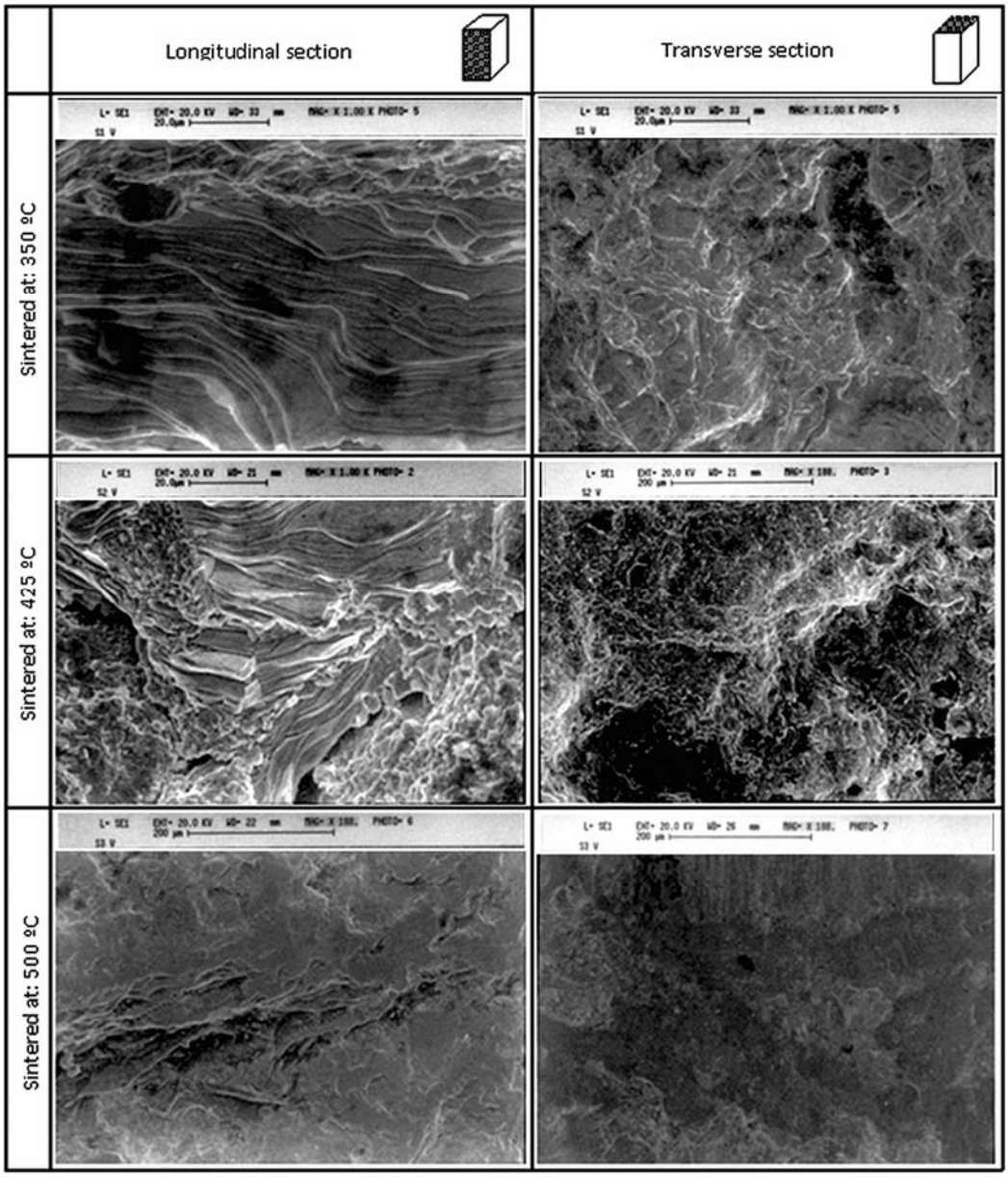

Figure 2. SEM microscopic images of microstructures of materials sintered at three typical temperatures: 350, 425 and 500°C, in both longitudinal and transverse directions.

3.1 *Material structure characterization*

Figure 1a shows powdered $(Bi_{0.25}Sb_{0.75})_2Te_3$ compound XRD pattern as a reference data. Figures 1b and c illustrate XRD patterns from both transverse and longitudinal sections of samples that were hot pressed at various sintering temperatures of 350, 425 and 500°C.

These patterns show that the alloy has a rhombohedral Sb_2Te_3 structure. The comparison of intensity and indices of patterns of sintered samples with those of the published X-ray diffraction data (figure 1a), will make it clear that the microstructures of all samples in longitudinal direction (figure 1c) are preferably orientated to (110) plane. However, in a transverse direction (figure 1b) at 500°C, not only strong diffraction peaks of the basal plane (110), but also (006) and (205) planes, were observed. This indicates that the microstructures of materials were preferably orientated to the basal plane at 500°C and the relative diffraction intensities are similar to those as referred to in the pulverizing result.

Morphology of the surfaces was studied by SPM that has used a NC–AFM mode. NC–AFM mode which is also referred to as a tapping mode characterizes the profile of brittle surface morphology and nanostructure of high precision (Kolodziej *et al* 2006; Xie 2007). Tapping on soft or brittle surfaces by thick probe oscillation of

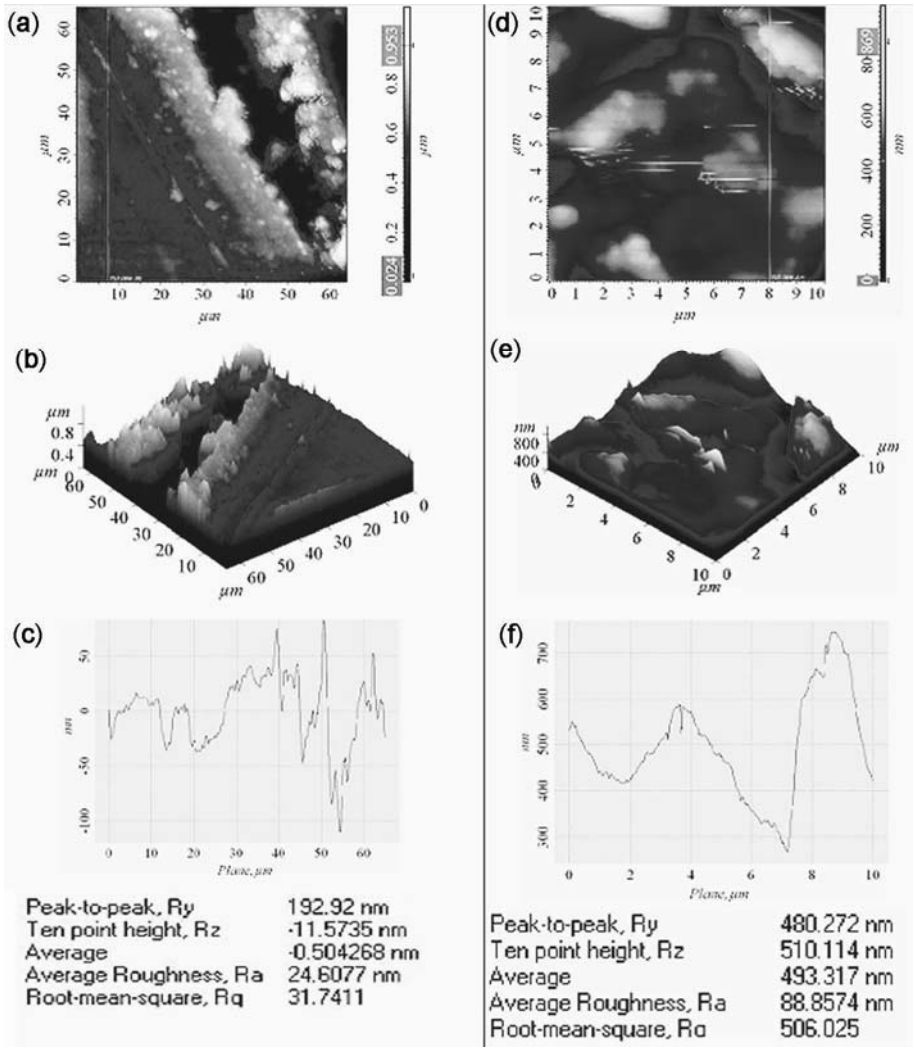

Figure 3. NC–AFM images from samples sintered at 500°C. The images were taken on 2D and 3D at 65 μm^2 and 10 μm^2 surface scan size from longitudinal direction. Profile of surface roughness is recorded along line shown on 2D images. From this roughness we can infer that grain boundaries are deformed under pressing.

appropriate NC–AFM tip prevents any damage to the surface by eliminating the lateral forces that are inherent in contact mode (where the tip is simply dragged over the surfaces). Providing a tip-sample contact area is at a minimum, the highest resolution (sub-nanometer) can be obtained in imaging non-periodic topographical features and the height on the images (z) also specified the most accurately true topography of soft samples (Wang *et al* 2003). Based on these definitions, force interaction between NC–AFM tip and the sample surface is minimized and the mode is suitable to acquire non-destructive imaging of more brittle samples.

SPM used in this study was Solver Pro (NT–MDT Ltd., Moscow, Russia) that operates in a tapping mode. The tip used was NC–G01S, which is compatible to most of SPM devices with nominal force constant, 5·5 N m^{-1}, at resonant frequency, 150 kHz. Images were manipulated by means of Flatten 2nd order processing software. AFM images were recorded from surfaces of the longitudinal and transverse sections of those samples which were taken off from the mold.

Microstructural texture can be clearly verified by viewing fracture surfaces of the materials as shown in figures 2–4. Figure 2 summarizes SEM images exposed microstructures in the samples that were sintered at three typical temperatures (350, 425 and 500°C) in both longitudinal and transverse directions. Images in longitudinal direction from the samples as sintered at different temperatures, especially those that have been sintered at lower temperatures demonstrate a layered structure, on the contrary to transverse direction, particularly those samples sintered at lower temperatures. Large cleaved flat grain facets were observed showing that basal planes (110) are well-matched with XRD results. Once sintered at 500°C,

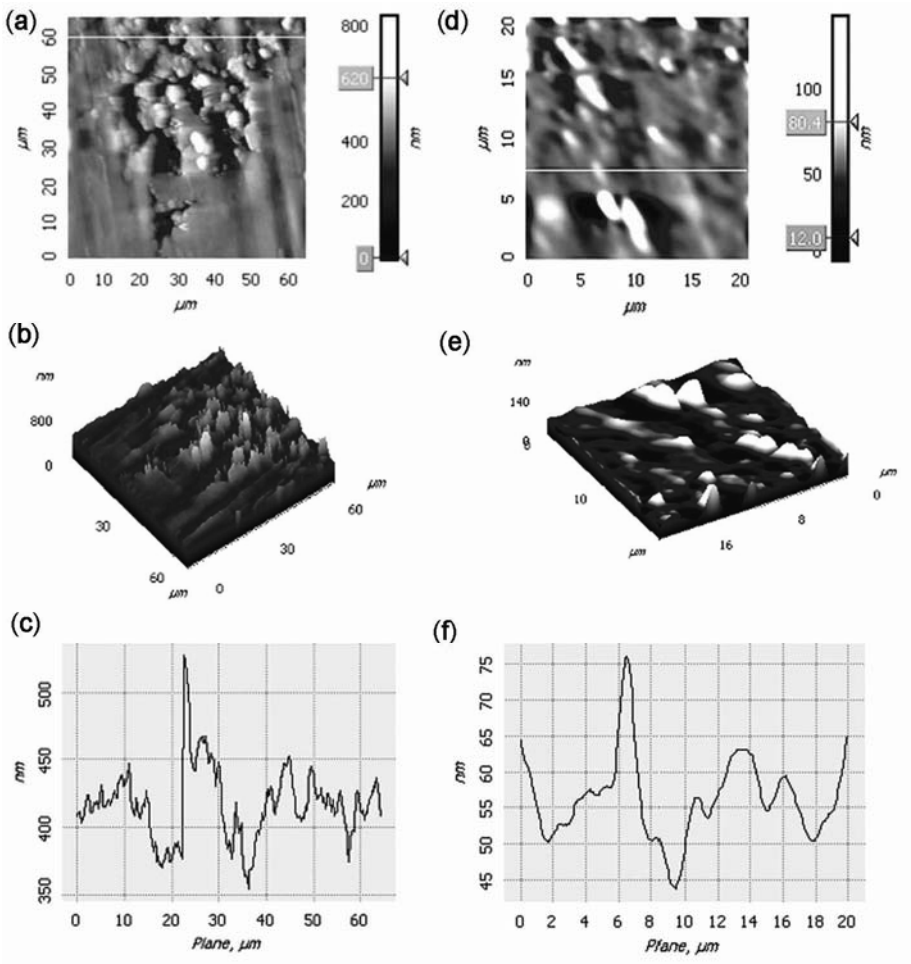

Figure 4. NC–AFM images of samples sintered at 500°C. Images were taken on 2D and 3D at 65 μm^2 and 20 μm^2 surface scan size from transverse direction. Profile of surface roughness is recorded along line shown on 2D images. From this roughness it can be deduced that the particles still have high self appearance on samples under 500 MPa pressure and 500°C.

grains were rather randomly oriented, and the grain size was lowered. These observations suggest that the dynamic recrystallization occurred during the sintering process at high temperatures.

SPM images validate these observations and suggest that grain boundaries were deformed in longitudinal direction for the samples sintered at 500°C under 500 MPa. In transverse direction particles in the size range 250–200 μm^2 were clearly observed. In order to visualize the particle size and size-distribution of crystallites in samples, the surfaces underwent different analyses. Figures 3c and 4c show section analysis along the lines shown in figures 3a and 4a for longitudinal direction and figures 3f and 4f show a section analysis along the lines shown in figures 3d and 4d for transverse direction, respectively.

Owing to the fact that powder (crystallites) was randomly filled into the mold for pressed sintered powder, considerable preferential orientation of an isotropic microstructure was expected to take place. However, the powder used in this study contained large size particles (under a sieving opening of 200 μm^2 and 250 μm^2) of platelet shapes, where the *c*-direction was perpendicular to the platelet. Apparently this platelet shape of the powders that were put into the mold and pressed resulted in the preferred orientation in transverse direction. In longitudinal direction it sounds rational that the particles with the basal planes bonded with Van der Waals' force will rotate perpendicular to the direction of the pressing load.

3.2 *Transport properties*

The thermal conductivity of a semiconductor is calculated by multiplying density, specific heat capacity and thermal diffusivity of the materials

$$\kappa = dC_p\kappa_d,$$

where d is the density, C_p specific heat capacity and κ_d thermal diffusivity of the material. While there is no rea-

son to prove the dependency of density and the specific heat capacity on orientation, the only factor which controls the orientation tendency of thermal conductivity is thermal diffusivity.

The thermal conductivity value that finds expression for ZT, contains electronic thermal conductivity, κ_{el}, lattice or phonon thermal conductivity, κ_L and the bipolar thermal conductivity, κ_b (Slack and Hussain 1991)

$$\kappa = \kappa_{el} + \kappa_L + \kappa_b.$$

As long as the bandgap E_g is ≥10 kT and according to approximate relationship, $E_g \approx 2e\alpha T$ (Slack and Hussain 1991), we can neglect κ_b, thus:

$$\kappa = \kappa_{el} + \kappa_L.$$

κ_{el} is related to electrical conductivity, σ, by the Wiedemann–Franz law:

$$\kappa_{el} = L_o \sigma T,$$

where $L_o \approx 3/2(k/e)^2$ is the Lorentz number and normally close to its classical value of $L_o = (1{\cdot}5–2{\cdot}45) \times 10^{-8}\ V^2\ K^{-2}$), for metals and semiconductors which varies with the level of doping, σ the electrical conductivity (Goldsmid and Sharp 1999) and T the absolute temperature. In order to have a chance of tendency for κ_{min}, the critical quantity that influences ZT is κ_L.

Considering the orientation tendency and as the sintering temperature largely depends on electrical conductivity, as discussed in our earlier paper (Kavei *et al* 2008b), it is evident that the κ_{el} part of thermal conductivity shows the same variation tendency under either orientation or sintering temperature. On the other hand, another part of the thermal conductivity, i.e. κ_L, is influenced by the grain size: the fine-grained microstructure contains larger quantity of specific grain boundaries which result in an accelerated phonon-grain boundary scattering, and give rise to reduced thermal conductivity (Goldsmid and Penn 1968; Parrot 1969). The results obtained in this study are consistent with this theory. That is, with an increase in the sintering temperature, particularly when sintered at a temperature higher than 425°C, the grain boundaries were reduced due to recrystallization. Reduction of grain boundaries resulted in a decrement in thermal conductivity, which is reflected by the moderate variation in thermal conductivity of the materials at higher part of the sintering temperature range. It sounds reasonable that even lower thermal conductivity can be achieved by further decrement in the grain boundaries. However, careful attention must be paid to the reduction of the grain boundaries for thermal conductivity decrement since it will simultaneously reduce the electrical conductivity of the material which may in turn bring about the effect of thermal conductivity reduction on the figure-of-merit. Small grain boundaries resulted in a decrement of Seebeck coefficient thermal and electrical conductivities; this is due to phonon and electron scattering by grain boundaries. An example of it has been given earlier (Martin-Lopez *et al* 1999) where Bi–Sb alloys were processed to contain fine grains. Despite the decrease in thermal conductivity, there is no improvement in the figure-of-merit because of excessive reduction in electrical conductivity.

Typical results of electrical conductivity of selected samples in longitudinal direction are 452 $(\Omega\ cm)^{-1}$ at 350°C, 523 $(\Omega\ cm)^{-1}$ at 425°C and 533 $(\Omega\ cm)^{-1}$ at 500°C. The measured values for thermal conductivity in longitudinal direction were 1·37, 1·46 and 1·53 at 350, 425 and 500°C, respectively. Table 1 also shows these values to allow comparison with those obtained by Keawprak *et al* (2005). Table 1 reveals that the compressive force has severe effect on the thermoelectric parameters; in particular, it increases the inexplicable value for thermal conductivity. The values are very high for thermoelectric elements and results in an inferior figure-of-merit. This is also due to oxidized thermoelectric elements and unwanted impurities which were entered while the rod was crushed and powdered. Although, we have obtained about $3 \times 10^{-3}\ K^{-1}$ for the same compound of thermoelectric in crystal form, but for sintered elements it was $Z = 1{\cdot}92 \times 10^{-3}\ K^{-1}$. Density of the samples was measured to be 6·43 g cm^{-3} with 0·29% water absorption and 1·86% apparent porosity at 350°C, 6·54 g cm^{-3} 425°C and 6·71 g cm^{-3} with 0·15% water absorption and 0·98 apparent porosity at 500°C.

4. Conclusions

After cleaning the surface of the samples with appropriate solver, a cylindrical rod of p-type thermoelectric material, $(Bi_{0{\cdot}25}Sb_{0{\cdot}75})_2Te_3$, was pulverized with particle size below 220 μm^2 [64% with a mesh of 80 (200 μm^2) and 36% with a mesh of 60 (250 μm^2)]. The obtained quantity of powder was pressed under 500 MPa axial pressure for 10 min, and then sintered at 350, 425 and 500°C (hot pressed). The material structure characteristics, transport and thermoelectric properties were studied and the following conclusions were drawn from the experimental data:

(I) After sintering, the microstructures of sintered samples were well aligned along the basal planes in a transverse direction, particularly when sintered at lower sintering temperatures (i.e. 350°C). However, an increased sintering temperature to 500°C reduced this preferential orientation in the microstructure substantially by recrystallization and reducing the available grain boundaries. Increased temperature results in a position in which a sample becomes stringent against brittleness.

(II) The compressive force magnitude, oxidized thermoelectric elements and unwanted impurities which entered into the powder have severe effect on the thermoelectric parameters, in particular, they increase inexplicable value for thermal conductivity. The value is high enough for

thermoelectric elements to result in an inferior figure-of-merit.

(III) In terms of figure-of-merit and strength of the sample, the optimum sintering temperature was 500°C leading to a maximum (Z) value of around $Z = 1{\cdot}92 \times 10^{-3}$ K^{-1} and strong enough to be used as a pellet.

(IV) Density of the samples depended on particle size and sintering temperature, small particle size resulted in an increment in density. This is reflected by the moderate variation in thermal conductivity of the materials at the higher part of the sintering temperature range.

References

Goldsmid H J and Penn A 1968 *Phys. Lett.* **A27** 523

Goldsmid H J and Sharp J W 1999 *J. Electron. Mater.* **28** 869

Hasezaki K, Nishimura M, Umata M, Tsukuda H and Araaoka M 1993 *Mechanical alloying of thermoelectric materials, Proc. 12th int. conf. on thermoelectrics (ICT, 12)* pp. 307–310

Hyun D B, Oh T S, Hwang J S and Shim J D 2001 *Scr. Mater.* **44** 455

Kavei G and Karami M 2006 *Bull. Mater. Sci.* **29** 659

Kavei G, Zare Y and Seyyedi A 2008a *J. Thermoelectr.* 57

Kavei G, Alinejad B, Kahramanov K Sh, Kazemzadeh A and Karami M A 2008b *J. Thermoelectr.* 31

Keawprak N Z M, Hashimoto H and Barsoum H M W 2005 *J. Alloys Compd.* **397** 236

Kitagawa H, Nagamori T, Tatsuta T, Kitamura T, Shinohara Y and Noda Y 2003 *Scr. Mater.* **49** 309

Kolodziej J J, Such B, Goryl M, Krok F, Piatkowski P and Szymonski M 2006 *Appl. Surf. Sci.* **252** 7614

Lide David R 2007–2008 *CRC handbook of chemistry and physics* (Boca Raton, FL: CRC Press) 88th edn, pp. 4-40–4-46

Liu Xue-Dong and Park Yong-Ho 2002 *Mater. Trans.* **43** 681

Martin-Lopez R, Dauscher A, Scherrer H, Hejtmanek J, Kenzari H and Lenoir B 1999 *Appl. Phys. A: Mater. Sci. & Process.* **68** 597

Oh T S, Hyun D B and Kolomoets N V 2000 *Scr. Mater.* **42** 849

Ohsugi I J, Kojima T and Nishida I A 1990 *J. Appl. Phys.* **68** 5692

Park K, Seo J H, Cho D C, Choi B H and Lee C H 2002 *Mater. Sci. Eng.* **B88** 103

Parrot J E 1969 *J. Phys.* **C2** 147

Scherrer H and Scherrer S 1995 *Bismuth telluride, antimony telluride, and their solid solutions, CRC handbook of thermoelectrics* (ed.) D M Rowe (Boca Raton: CRC Press) p. 211

Slack G A and Hussain M A 1991 *J. Appl. Phys.* **70** 2694

Wada H, Morimoto J, Miyakawa T and Irie T 1991 *Mater. Res. Bull.* **26** 179

Wang Y, Song R, Li Y and Shen J 2003 *Surf. Sci.* **530** 136

Xie H Y 2007 *China Particuology* **5** 242